Materials & Design 221 (2022) 110972

Contents lists available at ScienceDirect

Materials & Design

journal homepage: www.elsevier.com/locate/matdes

Effect of annealing on mechanical properties and thermal stability of ZrCu/O nanocomposite amorphous films synthetized by pulsed laser deposition

Francesco Bignoli [a,b,1], Saqib Rashid [c,1], Edoardo Rossi [c], Sahar Jaddi [d], Philippe Djemia [a], Giancarlo Terraneo [e], Andrea Li Bassi [b], Hosni Idrissi [d,f], Thomas Pardoen [d], Marco Sebastiani [c], Matteo Ghidelli [a,*]

[a] Laboratoire des Sciences des Procédés et des Matériaux (LSPM), CNRS, Université Sorbonne Paris Nord, 93430 Villetaneuse, France
[b] Dipartimento di Energia, Laboratorio Materiali Micro e Nanostrutturati, Politecnico di Milano, via Ponzio 34/3, I-20133 Milano, Italy
[c] Università degli studi Roma Tre, Engineering Department, via della Vasca Navale 79, 00146 Rome, Italy
[d] Institute of Mechanics, Materials and Civil Engineering (IMMC), UCLouvain, 1348 Ottignies-Louvain-la-Neuve, Belgium
[e] Laboratory of Supramolecular and Bio-Nanomaterials (SupraBioNanoLab), Department of Chemistry, Materials, and Chemical Engineering "Giulio Natta", Politecnico di Milano, Milano 20131, Italy
[f] Electron Microscopy for Materials Science, University of Antwerp, Antwerp, Belgium

HIGHLIGHTS

- Compact and nanogranular ZrCu/O films were deposited by pulsed laser deposition and annealed to investigate thermal stability.
- Nanogranular films crystallize at 300 °C, while the crystallization of compact films occurs >420 °C.
- The Young's modulus and hardness increase with annealing temperatures due crystallization process, reaching 180 and 14 GPa for nanogranular films.
- The residual stresses of compact films increase with annealing temperature, while for nanogranular ones they reach a maximum at 420 °C, indicating a complete crystallization.
- The evolution of structural/mechanical properties is studied, considering film morphology, local chemistry and free volume.

GRAPHICAL ABSTRACT

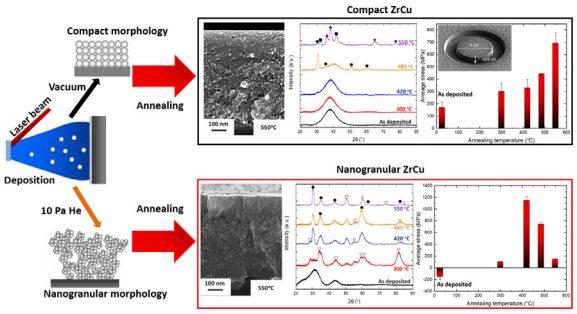

ARTICLE INFO

Article history:
Received 7 February 2022
Revised 6 July 2022
Accepted 19 July 2022
Available online 21 July 2022

Keywords:
Thin film metallic glasses

ABSTRACT

Binary ZrCu nanocomposite amorphous films are synthetized by pulsed laser deposition (PLD) under vacuum (2×10^{-3} Pa) and 10 Pa He pressure, leading to fully amorphous compact and nanogranular morphologies, respectively. Then, post-thermal annealing treatments are carried out to explore thermal stability and crystallization phenomena together with the evolution of mechanical properties. Compact films exhibit larger thermal stability with partial crystallization phenomena starting at 420 °C, still to be completed at 550 °C, while nanogranular films exhibit early-stage crystallization at 300 °C and completed at 485 °C. The microstructural differences are related to a distinct evolution of mechanical

* Corresponding author.
E-mail address: matteo.ghidelli@lspm.cnrs.fr (M. Ghidelli).
[1] These authors equally contributed to the article.

https://doi.org/10.1016/j.matdes.2022.110972

Pulsed laser deposition
Annealing treatments
Mechanical properties
Residual stress

properties and residual stress, with compact TFMGs showing the highest values of Young's modulus (157 GPa), hardness (12 GPa), strain rate sensitivity (0.096), and local residual stress (+691 MPa) upon annealing at 550 °C, while nanogranular films reach the maximum values of mechanical properties at 485 °C followed by relaxation at higher temperatures due to complete crystallization. We show that PLD in combination with post-thermal annealing can generate different families of amorphous films with varying nanoscale morphologies, resulting in tunable mechanical properties and thermal stability, which can thus be used for designing novel film configurations for different fields of application.

1. Introduction

Metallic glasses are characterized by many unique mechanical properties such as high yield strength (>2 GPa) and large elastic deformation (∼2 %) compared to crystalline metallic alloys counterparts [1–4]. However, they suffer from premature failure caused by the early formation of localized shear bands (SBs, ∼10 nm thickness) that propagate nearly instantaneously leading to catastrophic brittle fracture [5]. Nevertheless, this behavior can be mitigated by reducing the thickness of the metallic glass down to the submicrometer scale, activating mechanical size effects that could prevent the formation of SBs [6,7]. This finding paved the way to the study of thin film metallic glasses (TFMGs), showing homogenous deformation with suppression of SBs as well as an improvement of the mechanical properties [4,8], while leading to new paths for the development of nanostructured metallic glasses by adopting strengthening strategies so far applied for crystalline materials such as multilayer formation [9–11] and grain refinement in the so-called 'metallic nanoglasses' paradigm [12–14].

Recently, it has been discovered that pulsed laser deposition (PLD) enables the synthesis of a novel class of ZrCu nanocomposite amorphous films with a unique nanolayered structure, while controlling the morphology by simply changing the background gas pressure in the deposition chamber, resulting in the synthesis of compact or nanogranular films [15]. This results in a tunable mechanical behavior with a yield strength up to 3 GPa for compact films and ductility > 9 % for nanogranular films [15].

The mechanical properties and thermal stability of ZrCu TFMGs deposited by traditional methods like magnetron sputtering have been extensively studied by the articles of Apreutesei et al. [8,16], Zeman et al. [17] and Musil et al. [18].

However, the structural and mechanical properties of PLD-deposited nanocomposite amorphous films have not been deeply explored, especially regarding the effects of thermal treatments. Thermal treatments constitute the simplest way to enlarge the range of possible microstructures and properties that can be reached for a given composition. Usually, thermal treatment of bulk metallic glasses (BMGs) can be carried out above or below the glass transition temperature (T_g) [19,20]. Specifically, if the annealing is carried out at $T < T_g$, relaxation phenomena through free volume annihilation leave the atoms more closely packed, leading to a slight improvement of the mechanical properties [21]. Zhu et al. [22] performed nanoindentation on $Zr_{53}Cu_{36}Al_{11}$ after performing sub-*Tg* annealing at 553 K (0.8 T_g), reporting a slight enhancement of the hardness and Young's modulus from 5.6 and 99.2 GPa up to 6.1 and 105 GPa, respectively due to local densification. Similar results are reported by Gu et al. [21] for Cu_{36}-$Zr_{48}Al_8Ag_8$ BMGs, after annealing at 743 K for different times [21]. However, *in-situ* SEM compression test of micro-pillars reveal a mechanical brittle behavior for highly relaxed specimens, with a limited ductility [22]. This embrittlement is due to the reduced probability of nucleation of multiple shear bands due to the reduction of free volume [23]. This has been confirmed by Murali et al. [23] for bulk $Zr_{41.2}Ti_{13.75}Cu_{12.5}Ni_{10}Be_{22.5}$ with a maximum stress at fracture dropping from 11.2 down to 2.8 GPa after annealing at 500 K (0.8T_g).

On the other hand, annealing treatments performed above T_g lead to the growth of nanocrystals inside the amorphous matrix which can have both positive and detrimental effects [19,24]. In the work of Hajlaoui et al. [24], the fracture strain in compression of a ZrCu-based BMGs increases from 2 up to 10%, after a controlled annealing treatment generating a fine dispersion of nanocrystals. The ductilization is associated to the nucleation of multiple competing SBs which require high energy to percolate into a single band, while acting as deflectors and improving fracture toughness. On the other hand, Kumar et al. [19] found that crystallization severely embrittles BMG with the average fracture strain decreasing from 7.5 down to 1 % after annealing.

Despite these studies, a definitive understanding of the effects of annealing treatment on TFMGs remains a very open field. Additionally the PLD films possess a unique structure which could be affected by the annealing treatment in unexpected ways. Furthermore, there is no study which effectively includes the investigation of atomic and microstructure structure mechanical properties and residual stresses for such nanocomposite films as a function of the annealing treatment.

In the present work, we focus on the effects of annealing treatment (from 300 up to 550 °C) on thermal stability and devitrification process, by investigating the evolution of atomic structure in relationship with mechanical properties for ZrCu nanocomposites deposited by PLD with different initial microstructures. The structural and morphological properties of the films are investigated by X-ray diffraction (XRD), scanning electron microscopy (SEM) and atomic force microscopy (AFM). Brillouin light scattering (BLS) and nanoindentation are performed to determine the mechanical properties such as the elastic constants, hardness and strain rate sensitivity, while focused ion beam and digital image correlation (FIB-DIC) are used to extract local residual stresses. We show a different thermal stability behavior with compact films that have not completed their crystallization process while the nanogranular films are completely crystallized. Our results pave the way to the use of amorphous films possessing a combination of large mechanical properties and controlled thermal stability by simply tuning the deposition conditions and thermal treatment. Such materials will have large potential impact in the future as protective coatings to increase the wear resistance and fatigue life of engineering alloys as well as for the design of new stretchable electronics and memory storage systems such as resistive random access memory [25].

2. Materials and methods

2.1. Thin film deposition and annealing treatment

$Zr_{50}Cu_{50}$ (%at) thin films were deposited by ablating a $Zr_{50}Cu_{50}$ (99.99% pure, produced by 'MaTeck') target with a ns-pulsed laser (Nd:YAG, 1st harmonic, λ = 1064 nm, repetition rate 10 Hz, pulse duration 5–7 ns). The laser fluence on the target was set around

20.0 J/cm^2 and the laser pulse energy was 1850 mJ. Si (100) and soda lime glass were used as substrates after being cleaned in ultrasonic bath with isopropanol. The substrates were mounted on a rotating holder with a fixed distance from the target equal to 70 mm. All depositions have been carried out at room temperature in vacuum (2.1×10^{-3} Pa) or within a pure He atmosphere at a pressure of 10 Pa to induce respectively the formation of compact [26] and nanogranular cluster-assembled films [15,27]. The thickness of the films is ~800 nm, while the deposition rate was, respectively, equal to 1 and 1.3 nm/s for compact and cluster-assembled films. Post deposition thermal treatments were performed in a custom-made oven in high vacuum (7.0×10^{-5} Pa) with both ascending and descending thermal ramps equal to 10 °C/min and an isothermal dwell time equal to 1 h. The examined annealing temperatures were 300, 420, 485 and 550 °C.

2.2. Structural characterization

The crystallographic structure of the films was investigated by XRD using a θ-2θ Bruker D8 Advanced system with Cu Kα radiation (λ = 0.154 nm). The measurements were carried out in grazing incidence geometry with an incidence angle of 0.95° to avoid substrate signal with a scan range 20-90°. Data were acquired overnight by Lynx Eye detector in continuous scanning mode with a step size of 0.14°.

A field emission scanning electron microscope (FE-SEM) Zeiss Supra 40 equipped with energy dispersive X-ray spectroscopy (EDX) was used to perform morphological and elemental characterization of the films deposited on Si (100) substrates. The topography and surface average roughness (*Ra*) was characterized by using a Bruker atomic force microscope (AFM Dimension Icon, Bruker®, Billerica, MA, USA) operating in standard tapping mode. The AFM is equipped with a TESPA-V2 Bruker silicon probe featuring a nominal cantilever elastic constant of 42 N m^{-1} and a tip with a nominal radius of 8 nm. The AFM images were analyzed using the software Gwyddion®. The surface roughness was determined by measuring the average surface height of 10×10 μm^2 scans.

2.3. Mechanical characterization with Brillouin light scattering (BLS) and nanoindentation

In a BLS experiment, a monochromatic incident light beam is inelastically scattered by the thermally excited acoustic waves with a frequency shifted by ±*F* that can be analyzed with a Sandercock tandem Fabry-Pérot interferometer. The BLS spectra were obtained in air at room temperature with an incidence angle of 65° with acquisition times of 1 h and 200 mW of a p-polarized incident light (wavelength λ = 532 nm). For our opaque films, the scattering mechanism is restricted to the scattering of light by the dynamical corrugation of the free surface by surface acoustic waves (SAWs) travelling parallel to the film plane [28] and having a vertical displacement ($u_z(z = 0) \neq 0$). The sound velocity of SAWs is defined as $V_{SAW} = F\lambda/(2sin\theta)$. For our films, the Rayleigh surface wave (R) was observed. The Rayleigh sound velocity (V_R) is closely related to the transversal sound velocity V_T ($V_R \sim 0.92V_T$) [29]. From V_T, the shear modulus G (=C_{44}) can be obtained through the relationship $G = \rho V_T^2$ with ρ being the density of the film. From a fit of higher frequency (S_i), surface modes having a dispersive sound velocity V_{Si}, the second elastic constant C_{11} ($C_{11} = \rho V_L^2$) is extracted and then the longitudinal velocity, V_L (the information regarding the fits of the annealed ZrCu films can be found in the section 3 of the supplementary). Based on C_{11} and C_{44}, we can obtain the Young's modulus (E) of the film with the equation:

$$E = \frac{C_{44}(3C_{11} - 4C_{44})}{(C_{11} - C_{44})} \quad (1)$$

The BLS characterization is justified by its nondestructive nature to determine the elastic properties of our films without extrinsic effects from the substrate, enabling also independent assessment of the nanoindentation results.

Nanoindentation experiments have been carried out using a KLA-Nanomechanics G200 with a Berkovich diamond indenter operated in continuous stiffness measurement (CSM) mode to determine the Young's modulus (E) and hardness (H) as a function of the indentation depth. A standard fused silica sample was tested before and after the measurements for tip and frame stiffness calibrations. A minimum of 25 indentations were performed and the Oliver and Pharr model [30] was applied to extract E and H at indentation depth equal to 10 % of the film thickness [31].

The strain rate sensitivity (m) of the hardness has been calculated using $\partial lnH/(\partial ln\dot{\varepsilon})$ where $\dot{\varepsilon}$ is the representative indentation strain rate [2,32,33]. This strain rate can be estimated as equal to $\dot{P}/2P$ where $\dot{P}/P$ is the (constant) loading rate [32]. Three different loading rates equal to 0.02, 0.05, and 0.1 s^{-1} have been used. The activation volume (V_a) is equal to $3\sqrt{3}kT/mH$ where k is the Boltzmann constant, T is the test temperature and H is the mean hardness over the range of strain rates.

2.3.1. Residual stress measurements

The residual stress was determined combining focused ion beam and digital image correlation (FIB-DIC) micro-ring core method and using a specifically developed automated procedure within a FEI Helios Nanolab 600 dual beam FIB/SEM [34]. All the films were deposited with conductive gold particles (thickness ≈ 10 nm) by sputter coater (Emitech K550) to acquire better resolution SEM images with surface features, which are needed for DIC analysis. The pillar milling was performed using an annular trench with inner diameter of 6.5 μm, while employing a current of 48 pA with an acceleration voltage of 30 kV. The high-resolution secondary electron images were obtained before and after each milling step using an integral of 105 images at a dwell time of 50 ns. The milling process was carried out until the h/D ratio of 0.2 was achieved, where h and D represent the milling depth and the pillar diameter, respectively. The h/D ratio of 0.2 ensures an optimal strain relief, as demonstrated in Refs. [35,36]. After the milling cycle, all images were post-processed with a customized MATLAB based DIC code to determine the relaxation strain over the pillar [34]. Assuming an equi-biaxial stress distribution, the average stress σ in the film was calculated by using the interpolated relaxation strain at $h/D = 0.2$, E from the nanoindentation experiments and ν equal to 0.35 for compact films and 0.323 for nanogranular films according to the following relationship [37]:

$$\sigma = -\frac{E\Delta\varepsilon}{(1 - \nu)} \quad (2)$$

where $\Delta\varepsilon$ is the experimental relaxation strain at $h/D = 0.2$. The film thickness was also measured on the same micrographs adopted for the relaxation strain analysis. The step-by-step milling procedure, highlighting the different stages of milling process along with the film cross-section, is represented in Fig. 1.

3. Results and discussion

3.1. Structural and morphological properties

The X-ray diffraction patterns for compact and nanostructured ZrCu films deposited under vacuum and 10 Pa He are reported in Fig. 2a-b, respectively. Compact films are completely amorphous up to 300 °C with a hump positioned at ~38° in agreement with Apreutesei et al. [8] for ZrCu TFMGs deposited by sputtering. At 420 °C films are still mainly amorphous, but small peaks are

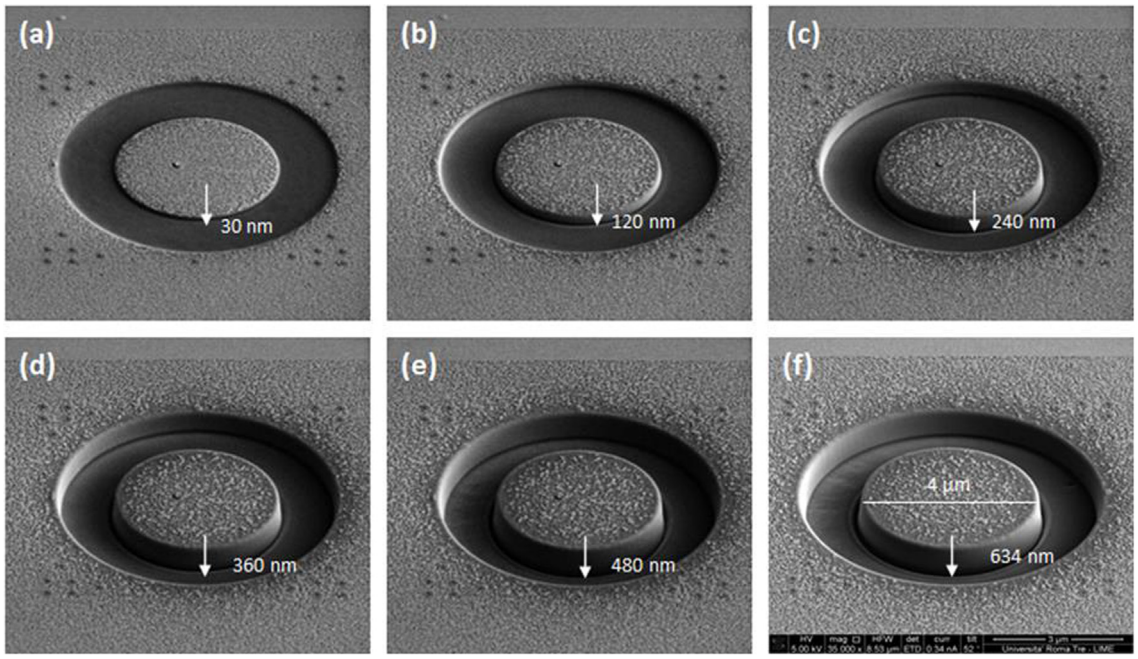

Fig. 1. Representative micrographs of as deposited compact films from (a) to (e) of the step-by-step milled pillar used to determine residual strain as a function of milling depth.

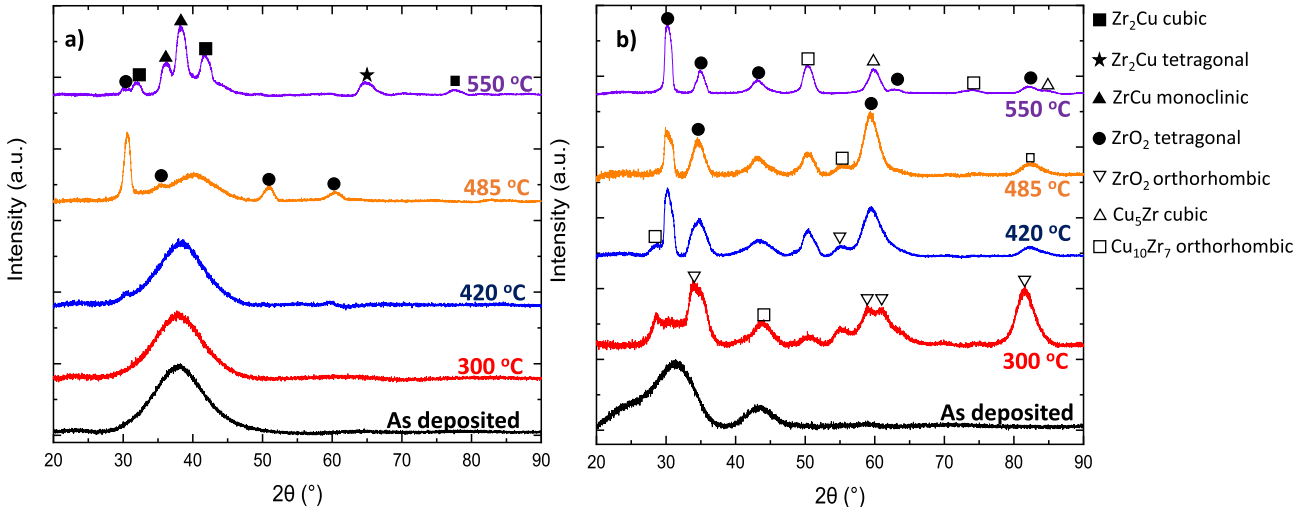

Fig. 2. XRD scans for compact (a) and nanogranular (b) ZrCu nanocomposite glass films annealed at different temperatures.

emerging at 30.3° and ~60° due to surface oxidation and thus the formation of tetragonal ZrO_2 [8]. Upon further annealing at 485 °C, four peaks related to the tetragonal phase of ZrO_2 appear together with amorphous hump, indicating a progressive depletion of the amorphous phase. The small shift of the amorphous hump position (at ~39°) can be associated to the depletion of Zr in the ZrCu amorphous matrix caused by the formation of ZrO_2 due to the slight presence of oxygen in PLD films which leaves a Cu-rich matrix with shorter bond distance respect to the as deposited matrix (see supplementary Fig. S1). The beginning of the crystallization process at T > 420 °C is in line with the works of Apreutesei et al. [8,16], reporting a crystallization temperature equal to 443 °C for ZrCu TFMGs deposited by magnetron sputtering with a similar composition. Finally, at 550 °C the film has completed the transition from amorphous to crystalline as observed by the disappearance of the amorphous hump and the formation of crystalline peaks related to monoclinic ZrCu, cubic Zr_2Cu and tetragonal Zr_2Cu, as expected for composition close to $Zr_{50}Cu_{50}$ [38] (see supplementary Fig. S2).

Fig. 2b shows the XRD spectra for nanogranular ZrCu deposited under 10 Pa He pressure. The as deposited film has two amorphous humps at 32° and 42.6° that can be related to a Zr-O rich phase (32°) and to a to Cu-rich ZrCu phase (42.6°) as already reported in Ref. [15]. The presence of several peaks at 300 °C suggests that formation a crystalline system which is composed by a complex mixture comprising zirconium oxide either as tetragonal and orthorhombic phases, a cubic phase of the Cu_5Zr and an orthorhombic phase of the $Cu_{10}Zr_7$ (see supplementary Fig S3). The appearance of crystalline peaks at a lower temperature with respect to compact films could be attributed to the presence of a nanogranular morphology of the films with larger free volume/interface content as well as by different local order. In fact the bond dilatation due to Zr-O rich layer can favor the nucleation of crys-

talline phases and atomic rearrangements upon heating [15]. Increasing the annealing temperature, namely from 420 up to 550 °C, the peaks related to tetragonal ZrO_2, cubic Cu_5Zr and orthorhombic $Cu_{10}Zr_7$ emerge without leaving any traces of amorphous matrix (whose diffraction hump is still visible at 300 °C). Upon crystallization, most of the Zr of the film has been converted in ZrO_2 with a small Cu_5Zr and $Cu_{10}Zr_7$ (see supplementary Fig S4, S5, S6). This is expected from the microstructure of these films as reported in Ref. [15] showing that nanogranular films contain a Zr-O rich phase.

Fig. 3 shows SEM cross-sections of compact and nanogranular ZrCu films as deposited and annealed up to 550 °C. Compact films (Fig. 3a) are produced in vacuum (2×10^{-3} Pa) due to the high kinetic energy of the ablated species also observed for the W crystalline materials of Ref. [39], while the film deposited at 10 Pa He (Fig. 3f) exhibits a nanogranular morphology as a result of in-plume cluster formation and cluster assembled growth [15]. After annealing, the compact films show corrugations patterns which are visible up to 420 °C (Fig. 3b-c) indicating that the films are still amorphous [40], although a few small crystalline features visible as small grains can be observed at 420 °C, in agreement with XRD (Fig. 2a). Finally, annealing at 485 and 550 °C (Fig. 3d,e) induces a change in the morphology of the film due to crystallization occurring at the expense of the amorphous matrix. On the other hand, for cluster-assembled films, the formation of crystalline phase is confirmed by the change in morphology starting at 420 °C (Fig. 3h). This indicates a lower thermal stability as a result of the larger free volume content, bond dilatation due to the high content of O in the Zr-O layers facilitating atomic redistributions at lower temperatures with respect to compact films, thus enabling the formation of thermodynamically stable crystalline phase at lower temperatures. Similar mechanisms were reported for nanoglasses showing a large free volume content with respect to compact glasses [13]. The ex-situ elemental characterization after annealing shows that the treatment does not cause any additional contamination of the film and that all atomic concentrations are equal to the ones of the as deposited films as in Ref. [15] (See supplementary Figure S7).

AFM scans of the upper surface of the compact and nanogranular ZrCu films are shown in Fig. 4 for the as deposited samples and the ones annealed at 550 °C, the images of the other annealed samples are presented in the supplementary (Figure S8, S9). AFM profiles for each film are presented in the supplementary information (Figure S10, S11). The surface of the films before annealing (Fig. 4 a, b) is very smooth with average roughness of 0.6 and 2.6 nm, respectively for compact and nanogranular nanocomposite glass films. The larger surface roughness of nanogranular films is related to the cluster-assembled growth regime and the high concentration of O that causes earlier nucleation of nanocrystalline grains and finally induces roughness to the film surfaces. The annealing treatment for both sets of ZrCu nanocomposite glass films leads to an increment of average surface roughness (Fig. 4e) due to the transformation of the amorphous phase into partially crystalline and completely crystalline at higher temperatures as shown in the XRD scans (Fig. 2). The surfaces roughness of compact films increases from 0.6 nm to 1.8 nm during annealing up to 420 °C (Fig. 4e) in which the films are still mainly amorphous due to nanocrystallization and the formation of small crystallites of ZrO_2. However, a further increase of the annealing temperature i.e. at 485 and 550 °C leads to more surface roughening, reaching 3.5 nm due to the nucleation and growth of crystalline grains (Fig. 4 c,e) [8]. A similar trend is observed for the nanogranular films in which the surface roughness increases from 2.6 up to 5.6 at 420 °C due to starting of crystallization. Then, when the annealing temperature reaches 485 and 550 °C, the surface roughness increases more rapidly from 8.5 up to 11.8 nm (Fig. 4d,e) [41]. The larger increment of roughness of the nanogranular films can be related to their larger free volume content and nanoscale interface density with a lower thermal stability with respect to the compact films, enabling a nucleation of a crystalline phase at lower temperatures [20].

3.2. Mechanical properties

Fig. 5 shows the variation of the shear modulus (G), Young's modulus (E), and hardness (H) as a function of annealing temperature as determined by Brillouin light scattering (BLS) and nanoindentation. The slight presence of O for as deposited compact films by PLD [15] is presumably responsible of the larger values with respect to the available literature data for ZrCu produced by sputtering, which usually have Young's modulus and hardness equal to 100 and 7 GPa respectively as found in Refs. [8,42]. Annealing treatments up to 420 °C induce no significant change in the mechanical properties, which then increase reaching the highest G, E and H values equal to 54, 157 and 12 GPa, respectively, at annealing temperature equal to 550 °C. As a matter of fact, compact nanocomposite glass films are still amorphous up to 420 °C and the following change of mechanical properties is due to the progressive formation of the crystalline phase, leading to an increase of around 15% of E and H similarly to the results of Ref. [43]. The continuous enhancement of the mechanical properties indicates that the crystallization process is not completed even at 550 °C as also demonstrated by XRD, showing the presence of an amorphous hump together with crystalline peaks (Fig. 2a).

Nanogranular films involve higher mechanical constants compared to the compact ones, with G, E and H reaching values up to 69, 180 and 14 GPa, respectively, after annealing at 550 °C. This corresponds to an increment by 25% with respect to the as deposited films, while such high values can be correlated with the high content of O inside the films which leads to the formation of a ZrO_2 phase, reporting large E and H [15,44]. However, nanogranular films show a marked growth from 300 to 400 °C followed by a plateau. This indicates an almost complete crystallization process at > 400 °C with a stable mechanical behavior as it has been shown in the XRD spectra. The values of Young's modulus (E) obtained by BLS are quite similar to the ones obtained by nanoindentation confirming the absence of artifacts caused by the substrate/surface during nanoindentation.

The rate sensitivity of the plastic deformation process has been investigated for compact films as a function of the annealing temperature (Fig. 5d). Both as deposited films and films annealed at 300 °C exhibit a strain rate exponent m equal to ~0.02 and apparent activation volume (defined as the volume of a material involved in the process of overcoming the energy barrier to form the shear bands) equal to ~100 Å^3 in agreement with literature values for Zr-based BMGs [32] and TFMGs deposited by sputtering [4]. This reflects the fact the specimens are amorphous without the formation of crystalline phases, while having a similar local order and free volume content [4,45]. Upon crystallization, the strain rate sensitivity progressively increases up to m = 0.10. This is an extremely large value involving a very small activation volume of ~20–30 Å^3. This is supported by the XRD analysis (Fig. 4a) in which it can be observed that the crystallization is not completed even at 550 °C with crystalline peaks emerging from the amorphous hump. As a matter of fact, crystallization induces a reduction of free volume through structural relaxation process leading to a decrease of the activation volume and the corresponding size of shear transformation zones (STZs) as found in Refs [22,32]. Moreover, such large values of m have also been found in monocrystalline Mg systems [46] as well as in $Zr_{75}Ni_{25}$ (m = 0.06) TFMGs in which the large amount of Zr (edge of amorphization) induces the reduction of

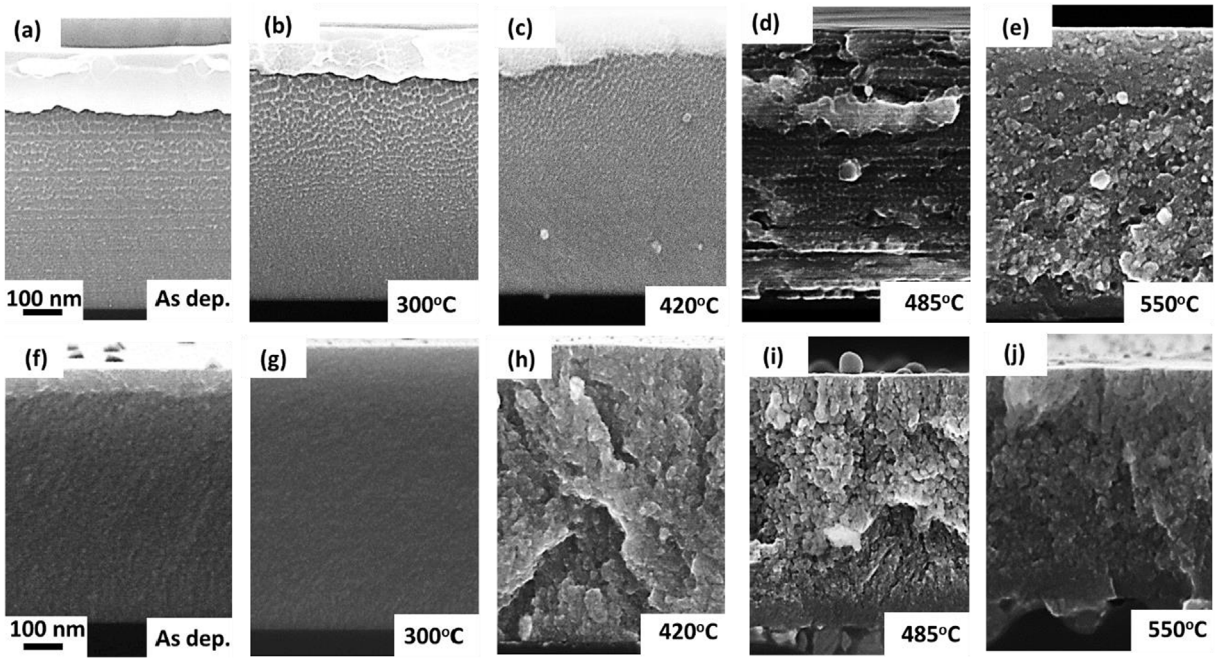

Fig. 3. SEM micrographs of as deposited compact (a) and nanogranular (f) ZrCu nanocomposite glass films. (b-e), (g-j) Morphological evolution upon annealing treatment from 300 up to 550 °C.

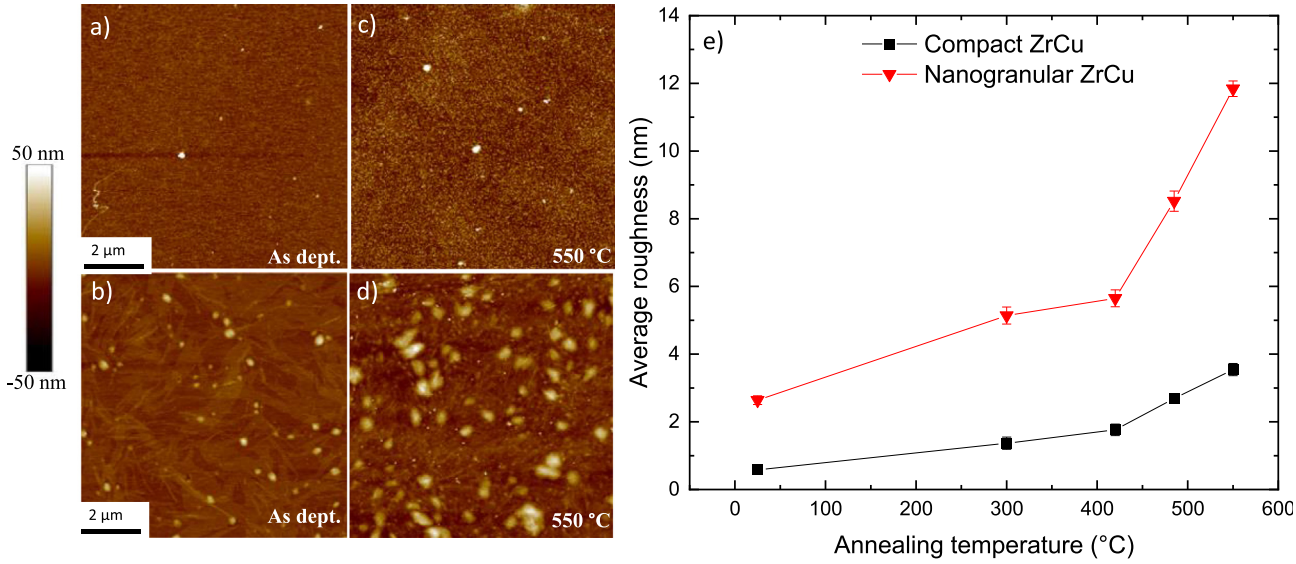

Fig. 4. (a,d) AFM scans for compact and nanogranular films as deposited and after annealing at 550 °C. (e) Evolution of the surface roughness of compact and nanogranular ZrCu nanocomposite glass films as a function of annealing temperature. (b,c).

mixing enthalpy and of activation volume as well as the formation of crystallites embedded within the amorphous matrix [4].

3.3. Residual stress measurement

Fig. 6 shows the relaxation strain for the ZrCu nanocomposite glass films determined by the FIB-DIC method. Positive relaxation strain corresponds to compressive stress and vice versa [35]. The variation of the strain as a function of depth represents a measure of the variation across the thickness of the residual stress state [35]. The residual stress comes from the thermal expansion mismatch between the film and the substrate as well as from microstructural evolution during film growth and atomic peening phenomena due to high energy of the ablated species as seen in the tungsten films of Ref. [47]. The relaxation strain for compact ZrCu films shows negative strain values throughout the entire thickness (Fig. 6a), which corresponds to a tensile residual stress state. On the other hand, the as deposited nanogranular ZrCu films show positive relaxation strain (compressive stress) which is shifted towards negative relaxation strain (tensile stress) after thermal treatment, as shown in Fig. 6b. The presence of compressive stresses in the as deposited films might be related to the contributions of background gas within the deposition chamber, affecting growth mechanisms due to lower energy of ablated spe-

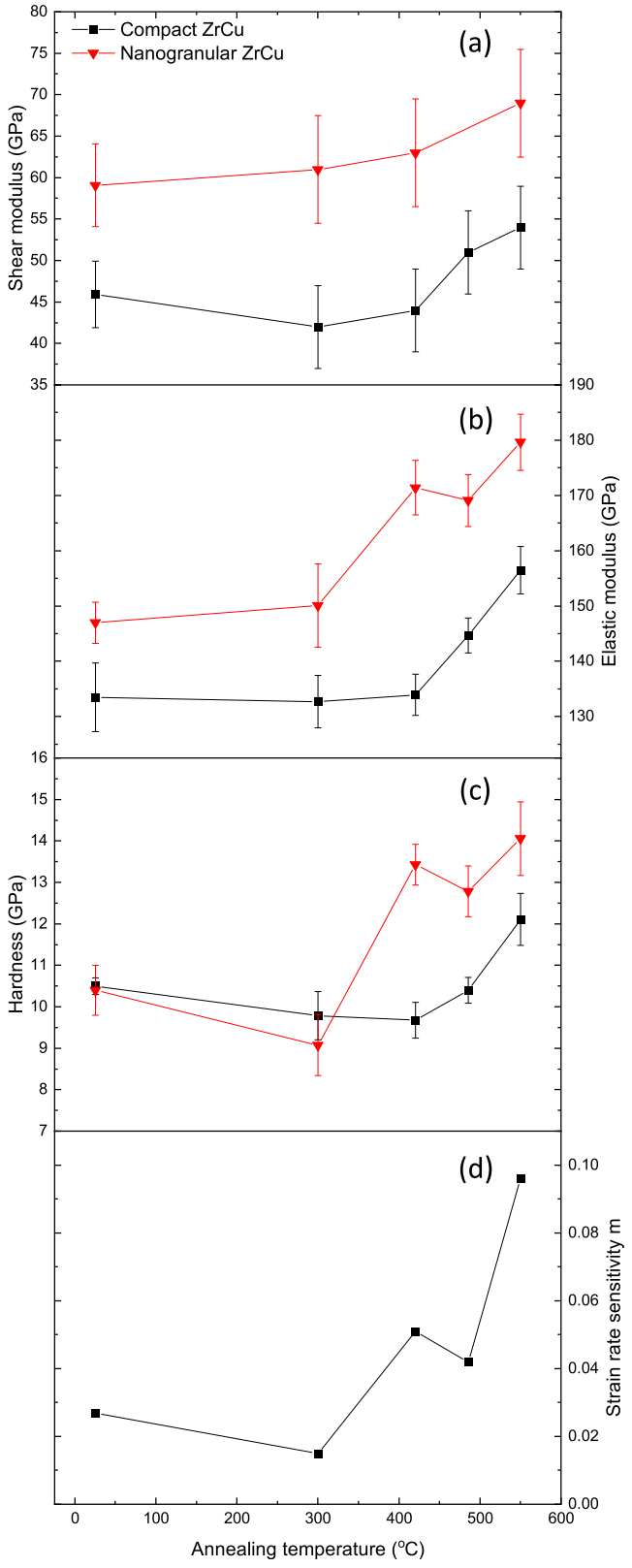

Fig. 5. Variation of shear (a) and Young's (b) moduli, (c) hardness and strain rate sensitivity (d) as a function of annealing temperature for compact and nanogranular ZrCu films.

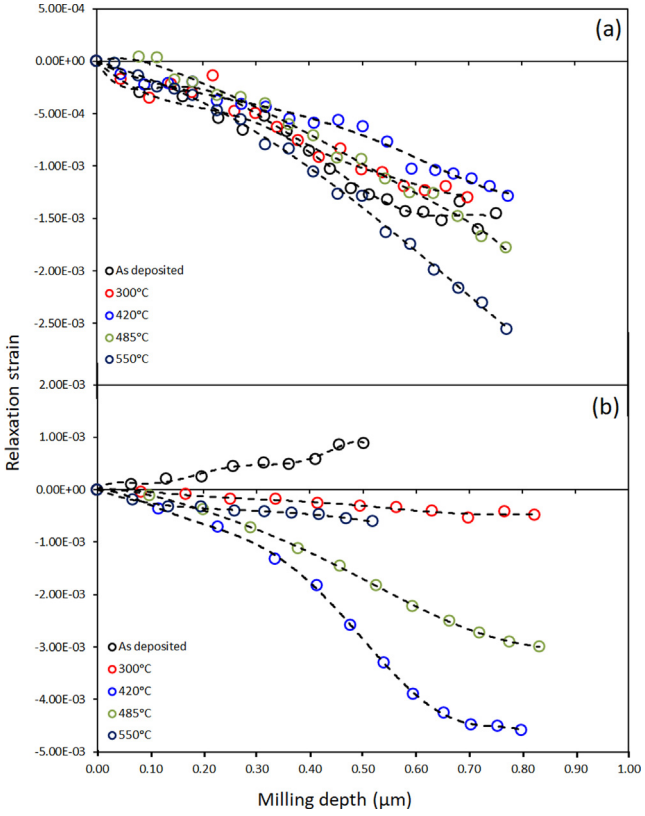

Fig. 6. Representative relaxation strain data sets, as determined by the FIB-DIC method for compact (a) nanogranular (b) ZrCu films as a function of milling depth.

cies [47]. The development of larger tensile stress can be initially caused by the annihilation of free volume and then from the nucleation and grain growth process related to the annealing temperature as reported in Ref. [48].

Besides the absolute values, also the slope of individual curves gives information about the stress evolution in the films. The relaxation strain of the compact ZrCu thin films annealed at temperature as high as 550 °C involves a larger slope as a function of the milling depth, indicating a higher residual stress gradient throughout the film thickness. This is likely associated to the polycrystalline nature of the film with higher annealing temperature promoting nucleation and crystal grain growth as also shown in Ref. [48].

The average residual stresses for ZrCu nanocomposite glass films as a function of annealing temperature are reported in Fig. 7. The compact films have residual stress increasing with annealing temperature from 169 up to 691 MPa. A similar result was found in the evolution of the residual stresses of FePt films of Ref [49], which can be qualitatively compared to the one reported in this work despite being purely crystalline. Such an increase is caused by the nucleation and crystalline grain growth during heating [48]. The presence of O inside metallic thin films has also been shown to increase the magnitude of tensile stresses inside thin films as observed in the papers by Shen et al. [50] and Yu *et al* [51] in which it is shown that different amounts of O can change the magnitude of tensile residual stresses from few hundreds of MPa to ~1 GPa.

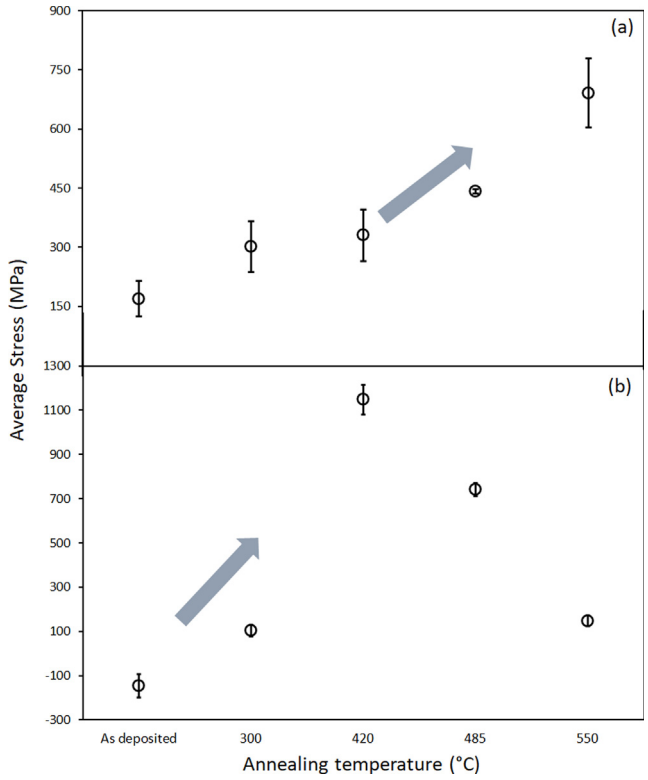

Fig. 7. Average residual stresses determined by the FIB-DIC method for compact (a) and nanogranular (b) ZrCu films as a function of annealing temperature.

Moreover, additional tensile stresses can develop during the cooling process after annealing treatment as a results of the mismatch between the coefficient of thermal expansion of the substrate and film [52]. An average tensile stress of 170 MPa is present in the as deposited compact ZrCu thin film, which approximately doubles up to 301–330 MPa while the structure remains amorphous at 300–420 °C. This can be caused by local atomic rearrangements, annihilation of free volume and relaxation. As the structure changes to partially crystalline at 485 °C, residual stresses increase up to 442 MPa to further reach a maximum of 691 MPa at 550 °C.

As deposited nanogranular films show a mild compressive residual stress equal to −146 MPa due to background gas collision and low kinetic energy of the ablated species, which changes to tensile (103 MPa) upon annealing at 300 °C due to crystal nucleation and growth. Further increasing the annealing temperature, an abrupt increment of tensile stress is reached up to 1148 MPa at 420 °C as the structure changes to fully crystalline. This maximum is followed by a subsequent drop (down to 148 MPa) of tensile stress with further increase in annealing temperature, a behavior already seen in the $PbTiO_3$ films of Ref. [53]. This trend can be explained by the crystallization occurring for cluster-assembled films which are less thermodynamically stable and containing an high amount of O which can increase the magnitude of tensile residual stresses to values as high as ∼1 GPa as observed in the works of Shen et al. [50] and of Yu et al. [51] on W and Ni films containing O, accompanied by stress relaxation after completing the crystallization process [41]. On the other hand, the continuous increment of residual stress observed for compact films with the annealing temperature can be related to the crystallization process which is still not completed, involving (nano)crystalline grains nucleation and growth from the amorphous phase as the ZnO films of Ref [54]. As a matter of fact, compact ZrCu TFMGs deposited by magnetron sputtering are known to have long crystallization kinetics with structural changes occurring even after 50 h at an annealing treatment of 700 K [55]. This is also supported by the continuous increment of the strain rate sensitivity with the annealing temperature as well as other mechanical properties with respect to nanogranular films.

4. Conclusions

ZrCu nanocomposite glass films produced by pulsed laser deposition (PLD) under vacuum and background gas pressure conditions, exhibit compact and nanogranular morphologies, respectively. Films were annealed at different temperatures from 300 °C up to 550 °C, leading to significant variations of the mechanical properties and thermal stability. The main findings of the work are:

- The formation of a large variety of micro- and nano-structures, including fully amorphous compact and nanogranular, amorphous embedded with nanocrystal, and fully crystalline by tuning annealing treatment at different temperatures. All films involve very smooth and crack-free surfaces with maximum average surface roughness ∼3.5 nm for compact films and up to 11.8 nm for nanogranular films owing to complete crystallization.
- Different thermal stability with compact films showing stable amorphous atomic structure up to 420 °C followed by partial crystallization at higher temperatures (T > 420 °C). On the other hand, nanogranular films show crystallization occurring already at 300 °C which is completed at 420 °C due to the high interface density, free volume and O content facilitating structural reorganizations, relaxation and nucleation of crystallites.
- Elastic moduli and hardness for both sets of films are larger than the values found in literature, due to the presence of O and increase with annealing temperatures due to the progressive atomic relaxation followed by the formation of crystallites as the microstructure transforms from amorphous to crystalline. However, the plateau reached for the nanogranular films indicates a complete crystallization process (even at 420 °C), while the continuous increment for compact ZrCu indicates a crystallization process not fully completed.
- Compact films show tensile stress increasing as a function of the annealing temperature (from 169 up to 691 MPa) due to relaxation and nanocrystalline phase nucleation followed by grain growth. On the other hand, nanogranular films show a maximum residual stress equal to ∼1148 MPa at 420 °C followed by a decrease at higher annealing temperatures, indicating a complete crystallization followed by stress relaxation.

The physical origin of these unique mechanical properties has been related to the local atomic order, free volume content, presence of O and film architecture (nanoclustering/interfaces), highlighting for the first time the mechanisms controlling mechanical properties and thermal stability for these new families of nanocomposite glassy films with engineered mechanical performances. These results pave the way to future scenarios for engineered films with tunable high structural performances, with key applications in the field of high resistance coatings for wear resistance, fatigue life improvement and also open new possibilities for the design of stretchable electronics and memory storage systems.

Data availability

The raw/processed data required to reproduce these findings cannot be shared at this time as the data also forms part of an ongoing study.

Declaration of Competing Interest

The authors declare that they have no known competing financial interests or personal relationships that could have appeared to influence the work reported in this paper.

Acknowledgements

M. Ghidelli and A. Li Bassi acknowledge the financial support of the Université Franco Italienne (UFI) for the funding of the PhD scholarship of F. Bignoli through a Vinci Cap. III Grant (#C3-2286). S. Rashid gratefully acknowledges partial financial support from the European Commission, European project Oyster, grant agreement no. 760827. M. Sebastiani gratefully acknowledges partial financial support from the European Commission, European project NanoMECommons, grant agreement no. 952869. Mechanical characterization activities were carried out at the "Inter-Departmental Laboratory of Electron Microscopy" (LIME), University of Roma Tre (http://www.lime.uniroma3.it). The Grant of Excellence Departments, MIUR (ARTICOLO 1, COMMI 314 – 337 LEGGE 232/2016) to the Department of Engineering, Università degli studi Roma Tre, is also gratefully acknowledged. H. Idrissi is mandated by the Belgian National Fund for Scientific Research (FSR-FNRS). This work was supported by the FNRS under Grants CDR – J.0113.20 and PDR - T.0178.19.

Appendix A. Supplementary data

Supplementary data to this article can be found online at https://doi.org/10.1016/j.matdes.2022.110972.

References

[1] M.F. Ashby, A.L. Greer, Metallic glasses as structural materials, Scripta Mater. 54 (3) (2006) 5.
[2] C.A. Schuh, T.C. Hufnagel, U. Ramamurty, Mechanical behavior of amorphous alloys, Acta Mater. 55 (12) (2007) 42.
[3] T. Egami, T. Iwashita, W. Dmowski, Mechanical Properties of Metallic Glasses, Metals-Basel. 3 (2013) 37.
[4] M. Ghidelli, S. Gravier, J.-J. Blandin, P. Djemia, F. Mompiou, G. Abadias, J.-P. Raskin, T. Pardoen, Extrinsic mechanical size effects in thin ZrNi metallic glass films, Acta Mater. 90 (2015) 232–241.
[5] A. Greer, Y. Cheng, E. Ma, Shear bands in metallic glasses, Mater. Sci. Eng. R Rep. 74 (4) (2013) 71–132.
[6] D. Tönnies, R. Maaß, C.A. Volkert, Room Temperature Homogeneous Ductility of Micrometer-Sized Metallic Glass, Adv. Mater. 26 (32) (2014) 5715–5721.
[7] H. Guo, P.F. Yan, Y.B. Wang, J. Tan, Z.F. Zhang, M.L. Sui, E. Ma, Tensile ductility and necking of metallic glass, Nat. Mater. 6 (10) (2007) 735–739.
[8] M. Apreutesei, P. Steyer, L. Joly-Pottuz, A. Billard, J. Qiao, S. Cardinal, F. Sanchette, J.M. Pelletier, C. Esnouf, Microstructural, thermal and mechanical behavior of co-sputtered binary Zr–Cu thin film metallic glasses, Thin Solid Films (561) (2014) 7.
[9] P.S. Zhen-Dong Sha, H.P. Branicio, T.E.T. Lee, Strong and ductile nanolaminate composites combining metallic glasses and nanoglasses, Int. J. Plasticity 90 (2017) 231–241.
[10] J.-Y. Kim, D. Jang, J.R. Greer, Nanolaminates Utilizing Size-Dependent Homogeneous Plasticity of Metallic Glasses, Adv. Funct. Mater. 21 (23) (2011) 4550–4554.
[11] G. Wu, Y. Liu, C. Liu, Q.-H. Tang, X.-S. Miao, J. Lu, Novel multilayer structure design of metallic glass film deposited Mg alloy with superior mechanical properties and corrosion resistance, Intermetallics 62 (2015) 22–26.
[12] X.L. Wang, F. Jiang, H. Hahn, J. Li, H. Gleiter, J. Sun, J.X. Fang, Plasticity of a scandium-based nanoglass, Scripta Mater. 98 (2015) 40–43.
[13] Y. Ivanisenko, C. Kübel, S.H. Nandam, C. Wang, X. Mu, O. Adjaoud, K. Albe, H. Hahn, Structure and properties of nanoglasses, Adv. Eng. Mater. 20 (12) (2018) 1800404.
[14] S.H. Nandam, Y. Ivanisenko, R. Schwaiger, Z. Śniadecki, X. Mu, D. Wang, R. Chellali, T. Boll, A. Kilmametov, T. Bergfeldt, Cu-Zr nanoglasses: Atomic structure, thermal stability and indentation properties, Acta Mater. 136 (2017) 181–189.
[15] M. Ghidelli, A. Orekhov, A. Li Bassi, G. Terraneo, P. Djemia, G. Abadias, M. Nord, A. Béché, N. Gauquelin, J. Verbeeck, J.-P. Raskin, D. Schryvers, T. Pardoen, H. Idrissi, Novel class of nanostructured metallic glass films with superior and tunable mechanical properties, Acta Mater. 213 (2021) 9.
[16] M. Apreutesei, P. Steyer, A. Billard, L. Joly-Pottuz, C. Esnouf, Zr–Cu thin film metallic glasses: An assessment of the thermal stability and phases' transformation mechanisms, J. Alloy. Compd. 619 (2015) 9.
[17] P. Zeman, M. Zítek, Š. Zuzjaková, R. Čerstvý, Amorphous Zr-Cu thin-film alloys with metallic glass behavior, J. Alloy. Compd. 696 (2017) 1298–1306.
[18] J. Musil, P. Zeman, Structure and microhardness of magnetron sputtered ZrCu and ZrCu-N films, Vacuum 52 (3) (1999) 269–275.
[19] G. Kumar, D. Rector, R. Conner, J. Schroers, Embrittlement of Zr-based bulk metallic glasses, Acta Mater. 57 (12) (2009) 3572–3583.
[20] X. Yi, W. Gao, B. Sun, H. Wang, D. Li, X. Meng, W. Cai, L. Zhao, The microstructure and mechanical properties of the as-spun and annealed ZrCu based ribbons, Appl. Surf. Sci. 481 (2019) 262–271.
[21] J. Gu, M. Song, S. Ni, S. Guo, Y. He, Effects of annealing on the hardness and elastic modulus of a Cu36Zr48Al8Ag8 bulk metallic glass, Mater. Design 47 (2013) 706–710.
[22] F. Zhu, S. Song, K.M. Reddy, A. Hirata, M. Chen, Spatial heterogeneity as the structure feature for structure–property relationship of metallic glasses, Nat. Commun. 9 (1) (2018).
[23] P. Murali, U. Ramamurty, Embrittlement of a bulk metallic glass due to sub-Tg annealing, Acta Mater. 53 (5) (2005) 1467–1478.
[24] K. Hajlaoui, A. Yavari, A. LeMoulec, W. Botta, F. Vaughan, J. Das, A. Greer, Å. Kvick, Plasticity induced by nanoparticle dispersions in bulk metallic glasses, J. Non-Cryst. Solids 353 (3) (2007) 327–331.
[25] P. Yiu, W. Diyatmika, N. Bönninghoff, Y.-C. Lu, B.-Z. Lai, J.P. Chu, Thin film metallic glasses: Properties, applications and future, J. Appl. Phys. 127 (3) (2020) 030901.
[26] P. Gondoni, M. Ghidelli, F. Di Fonzo, V. Russo, P. Bruno, J. Martí-Rujas, C.E. Bottani, A. Li Bassi, C.S. Casari, Structural and functional properties of Al:ZnO thin films grown by Pulsed Laser Deposition at room temperature, Thin Solid Films 520 (14) (2012) 4707–4711.
[27] B.R. Bricchi, M. Ghidelli, L. Mascaretti, A. Zapelli, V. Russo, C.S. Casari, G. Terraneo, I. Alessandri, C. Ducati, A. Li Bassi, Integration of plasmonic Au nanoparticles in TiO2 hierarchical structures in a single-step pulsed laser co-deposition, Mater. Design 156 (2018) 311–319.
[28] P. Djemia, F. Ganot, P. Moch, V. Branger, P. Goudeau, Brillouin scattering investigation of elastic properties of Cu–Mo solid solution thin films, J. Appl. Phys. 90 (2) (2001) 756–762.
[29] A. Kueny, M. Grimsditch, Surface waves in a layered material, Phys. Rev. B 26 (8) (1982) 4699.
[30] W.C. Oliver, G.M. Pharr, Measurement of hardness and elastic modulus by instrumented indentation: Advances in understanding and refinements to methodology, J. Mater. Res. 19 (1) (2004) 3–20.
[31] W.C. Oliver, G.M. Pharr, An improved technique for determining hardness and elastic modulus using load and displacement sensing indentation experiments, J. Mater. Res. 7 (6) (2011) 1564–1583.
[32] D. Pan, A. Inoue, T. Sakurai, M.W. Chen, Experimental characterization of shear transformation zones for plastic flow of bulk metallic glasses, Proc. Natl. Acad. Sci. U.S.A. 105 (39) (2008) 14769–14772.
[33] N. Van Steenberge, J. Sort, A. Concustell, J. Das, S. Scudino, S. Suriñach, J. Eckert, M. Baró, Dynamic softening and indentation size effect in a Zr-based bulk glass-forming alloy, Scripta Mater. 56 (7) (2007) 605–608.
[34] M. Sebastiani, C. Eberl, E. Bemporad, G.M. Pharr, Depth-resolved residual stress analysis of thin coatings by a new FIB–DIC method, Mater. Sci. Eng. A 528 (27) (2011) 7901–7908.
[35] M. Sebastiani, E. Rossi, M. Zeeshan Mughal, A. Benedetto, P. Jacquet, E. Salvati, A.M. Korsunsky, Nano-Scale residual stress profiling in thin multilayer films with non-equibiaxial stress State, Nanomaterials-Basel. 10 (5) (2020) 16.
[36] E. Salvati, L. Romano-Brandt, M.Z. Mughal, M. Sebastiani, A.M. Korsunsky, Generalised residual stress depth profiling at the nanoscale using focused ion beam milling, J. Mech. Phys. Solids 125 (2019) 488–501.
[37] F. Archie, M.Z. Mughal, M. Sebastiani, E. Bemporad, S. Zaefferer, Anisotropic distribution of the micro residual stresses in lath martensite revealed by FIB ring-core milling technique, Acta Mater. 150 (2018) 327–338.
[38] H. Okamoto, Cu-Zr (Copper-Zirconium), J. Phase Equilib. Diff. 33 (5) (2012) 417–418.
[39] E. Besozzi, D. Dellasega, A. Pezzoli, C. Conti, M. Passoni, M. Beghi, Amorphous, ultra-nano-and nano-crystalline tungsten-based coatings grown by Pulsed Laser Deposition: mechanical characterization by Surface Brillouin Spectroscopy, Mater. Design 106 (2016) 14–21.
[40] M. Ghidelli, S. Gravier, J.-J. Blandin, J.-P. Raskin, F. Lani, T. Pardoen, Size-dependent failure mechanisms in ZrNi thin metallic glass films, Scripta Mater. 89 (2014) 4.
[41] Y. Chen, Z. Zhu, H. Zhou, P. Ma, L. Lou, W. Zhu, G. Wang, Stress relaxation of three dimensional textured AlN films on sapphire substrate by rapid thermal annealing, Diam. Relat. Mater. 118 (2021) 108532.
[42] M. Apreutesei, C. Esnouf, A. Billard, P. Steyer, Impact of local nanocrystallization on mechanical properties in the Zr-59 at.% Cu metallic glass thin film, Mater. Design 108 (2016) 8–12.
[43] Y. Deng, Y. Guan, J. Fowlkes, S. Wen, F. Liu, G. Pharr, P. Liaw, C. Liu, P. Rack, A combinatorial thin film sputtering approach for synthesizing and characterizing ternary ZrCuAl metallic glasses, Intermetallics 15 (9) (2007) 1208–1216.
[44] J.J.R. Rovira, E.J. Piqué, M.A. Gomila, Nanoindentation of advanced ceramics: applications to ZrO2 materials, Applied Nanoindentation in Advanced Materials, John Wiley & Sons, Ltd, Chichester, UK (2017).

[45] H. Idrissi, M. Ghidelli, A. Béché, S. Turner, S. Gravier, J.-J. Blandin, J.-P. Raskin, D. Schryvers, T. Pardoen, Atomic-scale viscoplasticity mechanisms revealed in high ductility metallic glass films, Sci. Rep.-UK 9 (1) (2019).
[46] A. Pineau, A. Amine Benzerga, T. Pardoen, Failure of metals III: Fracture and fatigue of nanostructured metallic materials, Acta Mater. 107 (2016) 508–544.
[47] E. Besozzi, D. Dellasega, V. Russo, C. Conti, M. Passoni, M.G. Beghi, Thermomechanical properties of amorphous metallic tungsten-oxygen and tungsten-oxide coatings, Mater. Design 165 (2019) 107565.
[48] R. Daniel, K.J. Martinschitz, J. Keckes, C. Mitterer, The origin of stresses in magnetron-sputtered thin films with zone T structures, Acta Mater. 58 (7) (2010) 2621–2633.
[49] S.N. Hsiao, C.L. Chou, S.H. Liu, S.K. Chen, Influence of pressure on (0 0 1)-preferred orientation and in-plane residual stress in rapidly annealed FePt thin films, Appl. Surf. Sci. 509 (2020) 145304.
[50] Y. Shen, Y. Mai, Q. Zhang, D. McKenzie, W. McFall, W. McBride, Residual stress, microstructure, and structure of tungsten thin films deposited by magnetron sputtering, J. Appl. Phys. 87 (1) (2000) 177–187.
[51] H.Z. Yu, C.V. Thompson, Stress engineering using low oxygen background pressures during Volmer-Weber growth of polycrystalline nickel films, J. Vacuum Sci. Technol. A: Vacuum, Surf., Films 33 (2) (2015) 021504.
[52] W. Fang, C.-Y. Lo, On the thermal expansion coefficients of thin films, Sensor Actuat. A-Phys. 84 (3) (2000) 310–314.
[53] T. Ohno, H. Suzuki, D. Fu, M. Takahashi, T. Ota, K. Ishikawa, Effect of rapid thermal annealing on residual stress in lead titanate thin film by chemical solution deposition, Ceram. Int. 30 (7) (2004) 1487–1491.
[54] W.C. Lim, J.P. Singh, Y. Kim, J. Song, K.H. Chae, T.-Y. Seong, Effect of thermal annealing on the properties of ZnO thin films, Vacuum 183 (2021) 109776.
[55] D. Faurie, N. Girodon-Boulandet, A. Kaladjian, F. Challali, G. Abadias, P. Djemia, Setup for high-temperature surface Brillouin light scattering: Application to opaque thin films and coatings, Rev. Sci. Instrum. 88 (2) (2017) 7.